AJNR

Identification of Multiclass Pediatric Low-Grade Neuroepithelial Tumor Molecular Subtype with ADC MR Imaging and Machine Learning

Matheus D. Soldatelli, Khashayar Namdar, Uri Tabori, Cynthia Hawkins, Kristen Yeom, Farzad Khalvati, Birgit B. Ertl-Wagner and Matthias W. Wagner

Identification of Multiclass Pediatric Low-Grade Neuroepithelial Tumor Molecular Subtype with ADC MR Imaging and Machine Learning

Matheus D. Soldatelli, Khashayar Namdar, Uri Tabori, Cynthia Hawkins, Kristen Yeom, Farzad Khalvati, Birgit B. Ertl-Wagner, and Matthias W. Wagner

ABSTRACT

BACKGROUND AND PURPOSE: Molecular biomarker identification increasingly influences the treatment planning of pediatric low-grade neuroepithelial tumors (PLGNTs). We aimed to develop and validate a radiomics-based ADC signature predictive of the molecular status of PLGNTs.

MATERIALS AND METHODS: In this retrospective bi-institutional study, we searched the PACS for baseline brain MRIs from children with PLGNTs. Semiautomated tumor segmentation on ADC maps was performed using the semiautomated level tracing effect tool with 3D Slicer. Clinical variables, including age, sex, and tumor location, were collected from chart review. The molecular status of tumors was derived from biopsy. Multiclass random forests were used to predict the molecular status and fine-tuned using a grid search on the validation sets. Models were evaluated using independent and unseen test sets based on the combined data, and the area under the receiver operating characteristic curve (AUC) was calculated for the prediction of 3 classes: *KIAA1549-BRAF* fusion, *BRAF* V600E mutation, and non-*BRAF* cohorts. Experiments were repeated 100 times using different random data splits and model initializations to ensure reproducible results.

RESULTS: Two hundred ninety-nine children from the first institution and 23 children from the second institution were included (53.6% male; mean, age 8.01 years; 51.8% supratentorial; 52.2% with *KIAA1549-BRAF* fusion). For the 3-class prediction using radiomics features only, the average test AUC was 0.74 (95% CI, 0.73–0.75), and using clinical features only, the average test AUC was 0.67 (95% CI, 0.66–0.68). The combination of both radiomics and clinical features improved the AUC to 0.77 (95% CI, 0.75–0.77). The diagnostic performance of the per-class test AUC was higher in identifying *KIAA1549-BRAF* fusion tumors among the other subgroups (AUC = 0.81 for the combined radiomics and clinical features versus 0.75 and 0.74 for *BRAF* V600E mutation and non-*BRAF*, respectively).

CONCLUSIONS: ADC values of tumor segmentations have differentiative signals that can be used for training machine learning classifiers for molecular biomarker identification of PLGNTs. ADC-based pretherapeutic differentiation of the *BRAF* status of PLGNTs has the potential to avoid invasive tumor biopsy and enable earlier initiation of targeted therapy.

ABBREVIATIONS: AUC = area under the receiver operating characteristic curve; *FGFR* = fibroblast growth factors receptor; GG = ganglioglioma; GLMD = gray-level dependence matrix; ML = machine learning; NF1 = neurofibromatosis 1; NPV = negative predictive value; OvR = one versus the rest; PA = pilocytic astrocytoma; pLGG = pediatric low-grade glioma; PLGNT = pediatric low-grade neuroepithelial tumor; RF = random forests; WHO = World Health Organization

Pediatric low-grade neuroepithelial tumors (PLGNTs) are the most common pediatric CNS tumors, representing approximately 40% of all pediatric brain tumors.[1,2] According to the 5th Edition of the World Health Organization (WHO) classification, PLGNTs are grade 1 and 2 neoplasms described in 3 groups: diffuse pediatric low-grade gliomas (pLGGs), circumscribed astrocytic gliomas, and glioneuronal and neuronal tumors.[3] The genetic

and molecular features have been incorporated in this updated classification and, along with the histologic phenotype, relate to different prognoses and new targeted therapies.[4,5]

Most commonly, PLGNTs present with genetic changes causing upregulation of the Ras/mitogen-activated protein kinase (RAS/MAPK) pathway, usually fusions or mutations in the B-Raf proto-oncogene, serine/threonine kinase (BRAF) gene. The chromosomal alteration in BRAF fusion involves the duplication of the BRAF oncogene, followed by its insertion into one of several fusion targets, most often the K1AA1549 gene (KIAA1549-BRAF fusion).[6] BRAF V600E point mutations activate BRAF, causing deregulation in the mitogen-activated p.V600E protein kinase pathway.[7] Other common mutations include neurofibromatosis 1 (NF1), fibroblast growth factors receptors 1 and 2 (FGFR 1/2),[2,8] and MYB/MYBL1 rearrangements.[9-11] The most common histology for the KIAA1549-BRAF fusion and BRAF V600E mutation tumors is pilocytic astrocytoma (PA) and ganglioglioma (GG), respectively.[2,12] However, except for molecularly defined tumors, molecular subtypes are often found across various entities.[2,13]

Even though surgery is the preferred treatment for most PLGNTs when possible, more than one-half of PLGNTs cannot be completely resected, requiring subsequent pharmacologic therapy, often leading to high morbidity.[5,14] Genetic differences are essential for therapeutic decision-making, with BRAF and MEK inhibitors gaining popularity and new trials being developed.[15-17] Notably, BRAF inhibitors exhibit efficacy in BRAF V600E mutation tumors, while KIAA1549-BRAF fusion tumors might exhibit progression due to pathway paradoxic activation when treated with these inhibitors. Instead, KIAA1549-BRAF fusion tumors respond positively to MEK inhibitors.[15] However, implementing these new therapeutic strategies requires tissue sampling and molecular testing, mostly restricted to academic reference centers. Therefore, neuroimaging surrogates would be valuable tools for prognosis and treatment-planning.[2]

Radiomics has been applied to determine tumor histology, prognostication, and molecular classification (radiogenomics) in pediatric neuro-oncology.[18] Zhang et al[19] developed an MR imaging–based machine learning (ML) decision path that identified the 4 molecular subgroups of medulloblastomas. Wagner et al[17] demonstrated that FLAIR sequences predicted molecular subgroups of pLGG with a high area under the receiver operating characteristic curve (AUC) using a supervised ML approach. In addition, qualitative ADC features have recently been shown to predict BRAF V600E mutations among pLGGs.[16]

Despite the increased application of ML in pediatric neuroradiology, to date, there are no studies assessing radiomic features of ADC images in PLGNTs. Given the widespread use of ADC images and their relatively straightforward interpretation in the context of neoplastic cellularity and prognostication,[16] we hypothesized that KIAA1549-BRAF fusion, BRAF V600E mutation, and other non-BRAF PLGNTs can be differentiated quantitatively using the ADC map segmentations and that radiomics can improve diagnostic accuracy. Specifically, we aimed to develop and validate a radiomics ADC signature predictive of the molecular status of PLGNTs in pediatric patients using a bi-institutional cohort.

MATERIALS AND METHODS

Patients
This retrospective study was approved by the institutional review boards or research ethics boards of the 2 participating academic institutions: The Hospital for Sick Children, Toronto, Canada and Lucile Packard Children's Hospital, Stanford, Palo Alto, California. Due to the retrospective nature of the study, informed consent was waived by the local institutional review board/research ethics board. An interinstitutional data-transfer agreement was obtained for data-sharing. Patients were identified from the respective electronic health record database from January 2009 to January 2018. Patient inclusion criteria were the following: 1) 0–18 years of age, 2) availability of molecular information on BRAF status in histopathologically confirmed PLGNTs, and 3) availability of pretherapeutic brain MR imaging with non-motion-degraded FLAIR and DWI sequences, including ADC maps. Patients with spinal cord tumors were excluded.

Molecular Analysis
We used a targeted testing protocol. BRAF fusion status was determined using an nCounter Metabolic Pathways Panel (NanoString Technologies) or fluorescence in situ hybridization. BRAF p.V600E mutation was determined using immunohistochemistry, Droplet Digital (Bio-Rad Laboratories) polymerase chain reaction, as previously described.[14,20] For 233 patients, molecular analysis was performed with formalin-fixed paraffin-embedded tissue obtained during surgery. Nineteen patients had molecular subtyping based on frozen tissue. Fluorescence in situ hybridization was further used to detect MYB, MYBL1, and FGFR2 fused transcripts. Droplet Digital polymerase chain reaction was used to detect FGFR1 alteration, CDKN2A deletion, and IDH1 mutation. DNA sequencing was used for samples negative for our targeted testing protocol.

MR Imaging Acquisition, Data Retrieval, and Image Segmentation
Patients from the first academic institution (The Hospital for Sick Children, Toronto, Ontario, Canada) underwent brain MR imaging at 1.5T or 3T across various vendors (Signa, GE Healthcare; Achieva, Philips Healthcare; Magnetom Skyra, Siemens). Sequences acquired included axial DWI with ADC map calculation ($b = 0$ and 1000 s/mm^2, TR/TE, 6000–11,000/70–110 ms; 3- to 4-mm section thickness, 1 -to 3-mm gap), axial 2D T2 FLAIR, axial or coronal 2D T2-weighted FSE, and axial or sagittal 3D T1-weighted and axial or sagittal gadolinium-based contrast agent–enhanced T1-weighted sequences. Patients from the second academic institution (Lucile Packard Children's Hospital, Palo Alto, California) underwent brain MR imaging at 1.5T or 3T from a single vendor (Signa or Discovery 750; GE Healthcare). MR imaging was performed using the brain tumor protocol of the institution, which included 2D axial T2-weighted FSE, 2D axial or sagittal precontrast T1-weighted spin-echo, 2D axial T2 FLAIR, DWI with ADC calculation ($b = 0$ and 1000 s/mm^2, TR/TE, 7000–10,000/80–110 ms, 3- to 5-mm section thickness, 1- to 3-mm gap), and 2D axial gadolinium-based contrast agent–enhanced T1-weighted spin-echo sequences.

All MR imaging data were extracted from the respective PACS and de-identified for further analysis. Tumor segmentation
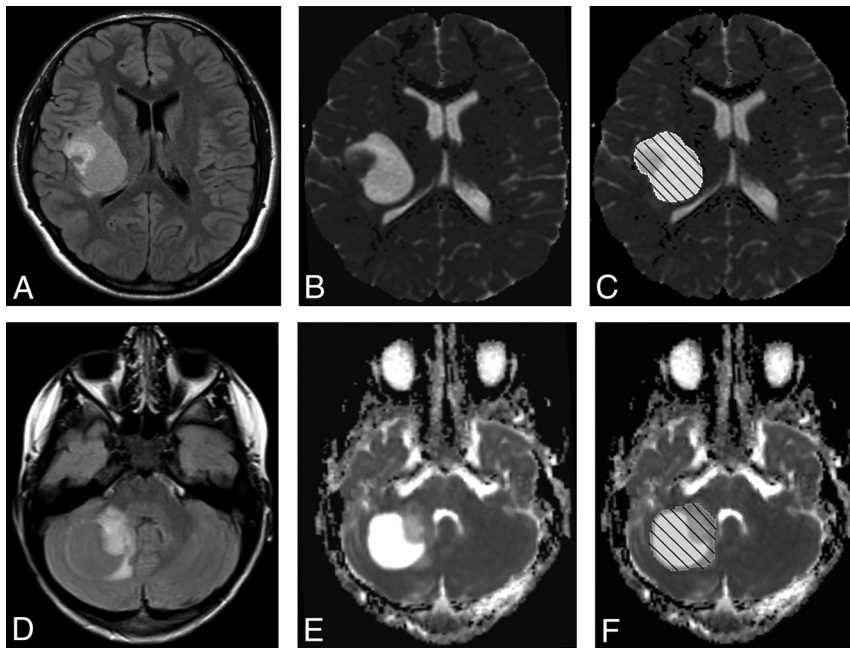
FIG 1. Axial FLAIR (*A* and *D*), ADC maps (*B* and *E*), and manual tumor segmentation using semiautomatic tools in 3D Slicer (*C* and *F*). Upper row: a 15-year-old adolescent boy with a supratentorial *BRAF*-mutated low-grade glioma. Lower row: a 3-year-old boy with a cerebellar *BRAF*-fused low-grade glioma.

was performed by a pediatric neuroradiology fellow with 3 years of neuroradiology research experience using 3D Slicer (Version 5.0.3; http://www.slicer.org).[21] Semiautomated tumor segmentation on ADC images was performed with the level tracing effect tool. Given that the tumors are better demonstrated on FLAIR images, these sequences were used as a guide to achieving the segmentation on the ADC images. The segmentation included both cystic and solid components of the tumor. This semiautomatic approach has been found superior to multiuser manual delineation concerning the reproducibility and robustness of results.[22] The senior author, a board-certified neuroradiologist, confirmed the final and proper placement of VOIs. Figure 1 demonstrates the segmentation process.

Radiomics Feature-Extraction Methodology

We used min-max normalization to scale the ADC images to [0, 1] and used the pyradiomics library with default hyperparameters to extract the radiomics features. A total of 688 radiomic features from the 3D VOIs in the ADC images were extracted for each patient. The radiomics features included shape, histogram, and texture features with and without wavelet-based filters. All features are listed in the Online Supplemental Data. Bias field correction was performed before segmentation to standardize the range of all image features.[23,24] Preprocessing and radiomics feature extraction in 3D Slicer and other software have been described elsewhere.[25-27] Clinical variables, including age, sex, and location, were appended to the data set.

Machine Learning and Statistical Analysis

We used random forests (RF) as the classification algorithm.[28] Previously, Wagner et al[29] demonstrated that RF perform best with limited data sets compared with other ML algorithms, including XGBoost (https://xgboost.readthedocs.io/en/stable/), and neural network architectures. The hyperparameter grid space was defined according to the Online Supplemental Data. We conducted 100 experiments and used an AUC to evaluate the classifiers. We randomly split our data into test (20%, 50 patients) and development (dev, 80%, 202 patients) sets in each iteration in a loop with N repetitions. Subsequently, a filtration algorithm was trained on the dev set and applied to the test set to eliminate highly correlated features (correlation coefficient >0.95). To measure the validation performance, models with the best hyperparameter set were trained and validated 100 times (N_val) on random dev data splits with a 75/25 ratio. Finally, an instance of the model with the best hyperparameters was trained on the entire dev set and evaluated on the test cohort. The whole process was repeated 100 times (N); thus, we have 100 test AUCs. The final evaluation of the model was conducted on the unseen test cohort.

We trained the RF classifiers in the supervised learning framework with 3 different inputs: 1) radiomics alone, 2) clinical variables (age, sex [binary], tumor location [binary]), and 3) radiomics and clinical variables together. A one versus the rest (OvR) multiclass AUC was used as the evaluation metric. Additionally, we monitored average per-class AUCs. We also captured the most meaningful features of the classifiers and selected the top 10 features across the experiments.

"Large p, Small n" is a well-known problem in ML, in which the number of features has a higher order in comparison with the number of examples. Radiomics-based ML is often affected by Large p, Small-n and is prone to overfitting. A crucial step is allocating an unseen cohort of data for test (compared with conventional methods such as standard cross-validation) to tackle the issue. To that end, we had separate train, validation, and test cohorts. In terms of feature selection, we filtered low-variance features (feature variance <0.05) and highly correlated features (correlation coefficient >0.95). Last, we repeated the experiments using different model initializations and data splits to ensure that the test performance was reproducible and overfitting was indeed avoided.

The analysis was conducted using Python 3.9.7 and scikit-learn 1.3.0 (https://scikit-learn.org/stable/index.html). For feature extraction, we used PyRadiomics 3.0.1 (https://pyradiomics.readthedocs.io/en/v3.0.1/changes.html) with SimpleITK 2.1.1.2 (https://simpleitk.org/doxygen/v1_0/html/).

RESULTS
Patients
The data of 422 patients were screened for inclusion. The data sets of 168 patients were excluded due to the absence of DWI-
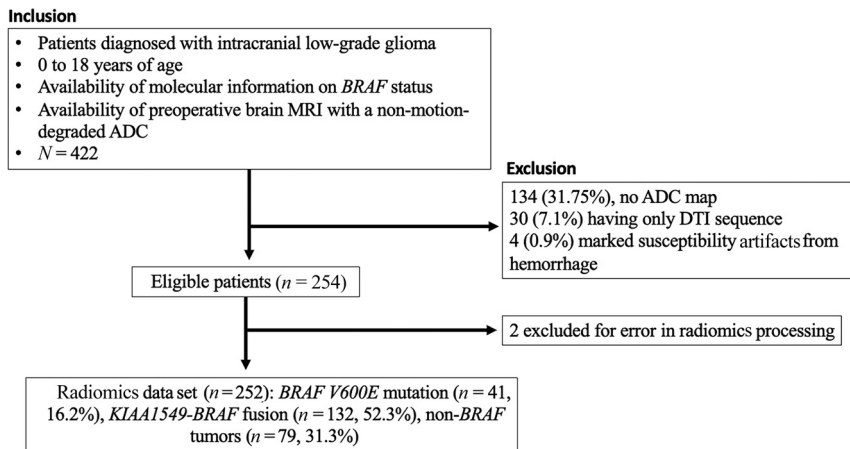
FIG 2. Flow chart of the study.

Table 1: Patient demographics

| | Institutional Cohort | | |
	Toronto	Stanford	Total
No. of patients	229	23	252
Age (mean) (yr)	8.18	6.32	8.01
Male (No.) (%)	124 (54.1%)	11 (47.8%)	135 (53.6%)
Histologic diagnosis (No.)			
PA	112	16	128
GG	24	5	29
LGA	36	0	36
PMA	8	2	10
PXA	4	0	4
DNET	10	0	10
DA	17	0	17
ODG	3	0	3
GNT	5	0	5
ACG	5	0	5
NC	1	0	1
DIG	1	0	1
PLNTY	1	0	1
Mixed tumor components	2	0	2
Molecular subgroup (No.) (%)			
KIAA1549-BRAF fusion	114 (49.7%)	18 (78.3%)	132 (52.2%)
BRAF V600E mutation	36 (15.7%)	5 (21.7%)	41 (16.6%)
Non-BRAF	79 (34.4%)	0	79 (31.2%)
Supratentorial (No.) (%)	125 (54.5%)	5 (21.7%)	130 (51.8%)
Infratentorial (No.) (%)	104 (45.4%)	18 (78.3%)	122 (48.2%)

Note:—ACG indicates angiocentric glioma; DA, diffuse astrocytoma; DIG, desmoplastic infantile ganglioglioma; DNET, dysembryoplastic neuroepithelial tumor; GNT, glioneural tumor; LGA, low-grade astrocytoma; NC, neurocytoma; PMA, pilomyxoid astrocytoma; PXA, pleomorphic xanthoastrocytoma; PLNTY, polymorphous low-grade neuroepithelial tumor of the young; ODG, oligodendroglioma.

derived ADC images (134 for not having ADC maps and 30 for having DTI). Four patients were excluded due to marked susceptibility artifacts from hemorrhage, and 2 were excluded for errors in radiomics processing (Fig 2). After all preprocessing and radiomics extraction steps, 252 patients were included (first institution, $n = 229$, second institution, $n = 23$), comprising 135 boys (53.6%); mean age, 8.01 (SD, 4.88) years. Patient demographics and pathologic information consisting of age, sex, histologic diagnosis, *BRAF* molecular status, and anatomic location of the tumor (supra-versus-infratentorial) are shown in Table 1.

Among the non-*BRAF* tumors ($n = 79$, 31.2%), we identified the following molecular markers: *FGFR1* ($n = 10$, 3.9%), NF1

($n = 5$, 2%), *MYB* proto-oncogene like 1 (*MYBL1*) ($n = 4$, 1.6%), *MYB* proto-oncogene (*MYB*) ($n = 4$, 1.6%), *FGFR2* ($n = 2$, 0.8%), isocitrate dehydrogenase 1 (*IDH1*) ($n = 2$, 0.8%), *histone H3.3 K27M* ($n = 2$, 0.8%), transforming acidic coiled-coil containing protein 1 (*TACC1*) ($n = 2$, 0.8%), platelet-derived growth factor receptor α (*PDGFRA*) ($n = 2$, 0.8%), *PIK3CA* ($n = 2$, 0.8%), *QKI-RAF1* ($n = 2$, 0.8%), as well as a single case (0.4%) of anaplastic lymphoma kinase (*ALK*), neurotrophic tyrosine receptor kinase (*NTRK*), *MYB-QKI* rearrangement, mitogen-activated protein kinase 1 (*MAPK1*), chloride voltage-gated channel 6 (*CLCN6*), *FYCO-RAF1*, G protein subunit α 11, and *GOPC-ROS1*. In addition, cyclin-dependent kinase inhibitor 2A (*CDKN2A*) gene deletions were identified in 29 tumors (11.5%): 12 *KIAA1549-BRAF* fusions (4.76%), 7 *BRAF* V600E mutations (2.77%), and 10 non-*BRAF tumors* (3.96%).

Radiomics Model Evaluation

Given that one of our cohorts did not have 1 tumor subtype, the bi-institutional cohort was analyzed together, and 252 patients were randomly split into 80% development and 20% test cohorts in each experiment, as illustrated in the radiomics pipeline in Fig 3. We used 3-class classifiers and achieved the following results (OvR, AUC) over 100 experiments (different data splits).

The top discriminative features are shown in Table 2. We encountered the first-order and gray-level dependence matrix (GLMD) classes among our top discriminative features. The mean, kurtosis, and 90th percentile in this class differ among the 3 subgroups. In addition, the dependence variance, large dependence emphasis, and large dependence high gray-level emphasis differed among our subgroups. The most important clinical feature was tumor location (supra- and infratentorial).

Figure 4 shows the average AUC across all groups. By means of only the radiomics features, the average test AUC was 0.74 (95% CI, 0.73–0.75) using the OvR method. When the input was restricted to clinical features, the average test AUC dropped to 0.67 (95% CI, 0.66–0.68). The combination of both radiomics and clinical features improved the predictive performance to an AUC of 0.77 with (95% CI, 0.75–0.77).

The diagnostic performance of the per-class test AUC in identifying *KIAA1549-BRAF* fusion, *BRAF* V600E mutation, and non-*BRAF* tumors among the other subgroups is shown in Table 3. It was higher in identifying *KIAA1549-BRAF* fusion tumors among the other subgroups (AUC = 0.81 for the combined radiomics and clinical features versus 0.75, 0.74 for *BRAF* V600E mutation, and non-*BRAF*, respectively).

DISCUSSION

Using a bi-institutional cohort, we trained and tested radiomics models predictive of *KIAA1549-BRAF* fusion, *BRAF* V600E mutations, and non-*BRAF* alterations in PLGNTs. The optimal

RF model achieved an accuracy AUC of 0.77 when combining radiomics and clinical features. In addition, we showed that the diagnostic performance was higher in differentiating *KIAA1549-BRAF* fusion from *BRAF* V600E mutation and non-*BRAF* tumors, regardless of which features were used (radiomics, clinical, and combined). To our knowledge, this is the first study that investigated ADC-based radiomics features in PLGNTs.

PLGNTs are a heterogeneous group of tumors arising predominantly from the glial cell lineage, including astrocytic, oligodendrocytic, or mixed neuronal and glial lineage.[9] These neoplasms are classified as WHO grades 1 and 2 and are grouped into 3 categories in the fifth WHO classification: circumscribed astrocytic gliomas, glioneural and neuronal tumors, and pediatric-type diffuse low-grade gliomas (those with characteristic ill-defined infiltrative margins).[3] PAs are the most common well-circumscribed PLGNT (up to 85%) and are by far the most common brain tumor type with *KIAA1549-BRAF* fusion. Therefore, the *KIAA1549-BRAF* fusion is a useful putative diagnostic
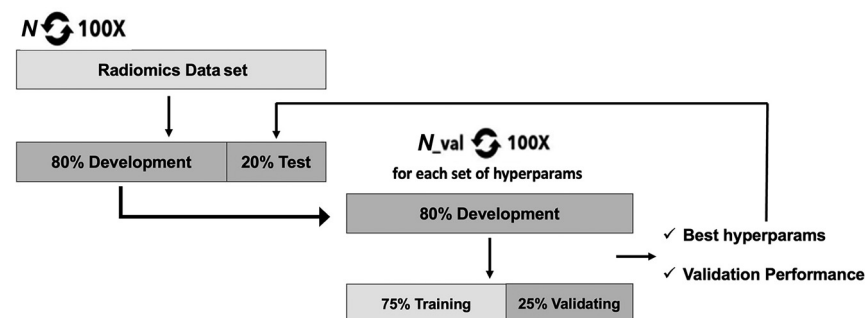

FIG 3. The repetitive classification approach.

Table 2: Top predictive radiomics and clinical features

| Type	Source	Feature Category	Feature
Clinical	NA	NA	Tumor location
Radiomics	3D wavelet transform	Gray-level difference matrix	Large dependence high gray-level emphasis
Radiomics	3D wavelet transform	First order	Mean
Radiomics	3D wavelet transform	First order	Kurtosis
Radiomics	Original	Gray-level difference matrix	Dependence variance
Radiomics	Original	Gray-level difference matrix	Large dependence high gray-level emphasis
Radiomics	Logarithm	Gray-level difference matrix	Large dependence high gray-level emphasis
Radiomics	Local binary pattern 3D	Gray-level difference matrix	Large dependence emphasis
Radiomics	Exponential	First order	90th Percentile
Radiomics	3D wavelet transform	First order	Kurtosis

Note:—NA indicates not applicable.
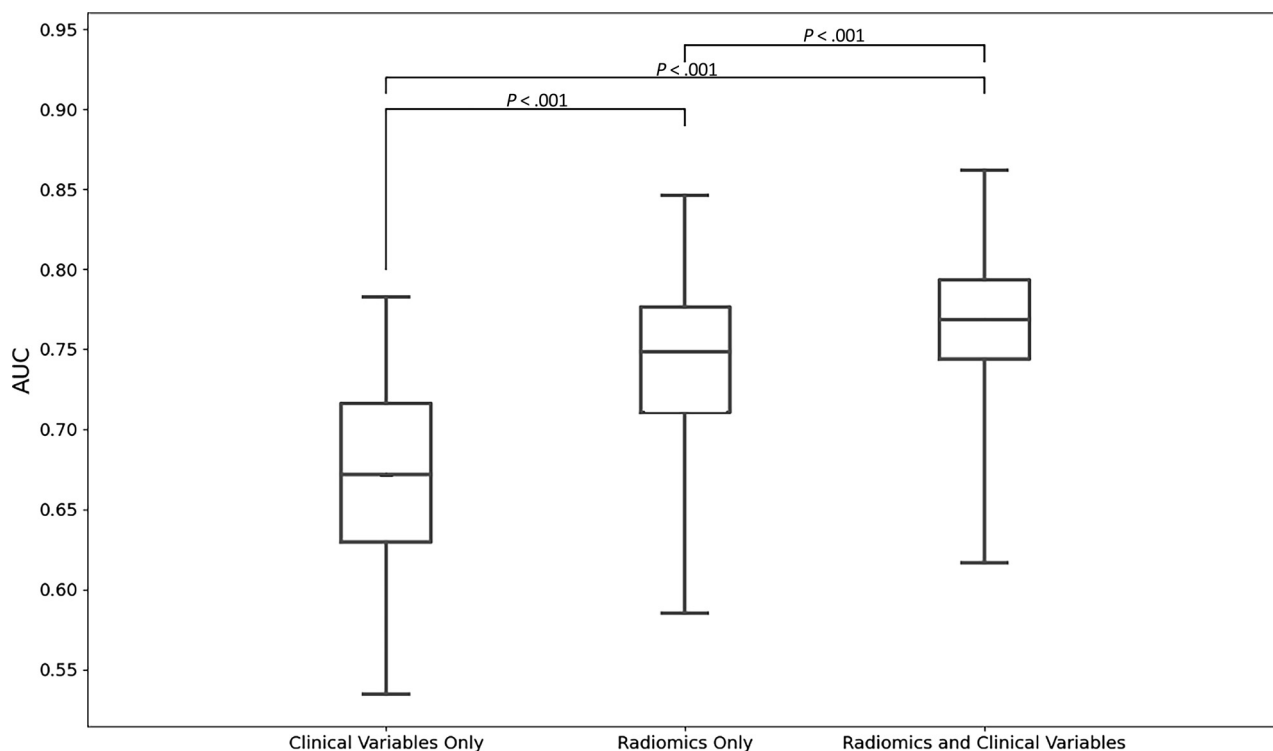
FIG 4. Boxplots of test AUCs. Note that *P* values are calculated on the basis of Student *t* tests.

Table 3: Per-class and overall OvR test of AUC performance of the models

	KIAA1549-BRAF Fusion versus the Rest	*BRAF* V600E Mutation versus the Rest	Non-*BRAF* versus the Rest	Average
Radiomics features only	AUC = 0.80 95% CI, 0.79–0.81	AUC = 0.74 95% CI, 0.73–0.75	AUC = 0.67 95% CI, 0.66–0.68	AUC = 0.74 95% CI, 0.73–0.75
Clinical features only	AUC = 0.75 95% CI, 0.74–0.7	AUC = 0.62 95% CI, 0.61–0.63	AUC = 0.63 95% CI, 0.62–0.6	AUC = 0.67 95% CI, 0.66–0.68
Combined radiomics and clinical features	AUC = 0.81 95% CI, 0.81–0.82	AUC = 0.75 95% CI, 0.73–0.75	AUC = 0.74 95% CI, 0.672–0.74	AUC = 0.76 95% CI, 0.75–0.7)

marker, particularly for PAs, which can show the neuropathologic features of necrosis and microvascular proliferation, also seen in high-grade gliomas.[30] The *BRAF* V600E mutation, on the other hand, is present in a more heterogeneous group of neoplasms with a worse prognosis, such as GG, dysembryoplastic neuroepithelial tumors, pleomorphic xanthoastrocytomas, astroblastomas, and diffuse low-grade gliomas *MAPK* pathway-altered.[31] These 2 *BRAF* tumor subgroups also differ clinically because those with the V600E mutation tend to be supratentorial, while those with *KIAA1549-BRAF* fusion are usually located in the brainstem or cerebellum.[9]

DWI reflects the free movement of water molecules in tissue.[32] Highly cellular tumors often show decreased ADC values.[33] Most studies use ROI analysis to evaluate brain tumors,[34] though it represents only a part of the lesion and is highly subjective. A better alternative is ADC histogram calculation, which analyzes the entire lesion and may show tissue heterogeneity;[35] however, this technique is limited because different tissue components may have overlapping signal intensities.[36] Alternatively, ML classifiers using radiomics features can extract data from larger volumes of images, increasing reproducibility, providing signatures in different CNS neoplasms, and assessing therapeutic interventions.[36-39] ML models are associated with randomness; and especially with small data sets, it is crucial to measure the randomness of the models. Additionally, the reproducibility of radiomics studies is a major concern that demands a systematic evaluation. In this research, we followed the OpenRadiomics (https://arxiv.org/abs/2207.14776)[38,40] protocol to achieve reproducible results.

Ramaglia et al[41] first described the association between *BRAF* V600E and lower relative ADC values. Similar diagnostic performances were predicted by different parameters, such as relative ADC mean (AUC = 0.83, $P < .001$) and relative ADC minimum (AUC = 0.85, $P < .001$).[41] Trasolini et al[16] and Shrot et al[35] also reported the association of *BRAF* V600E and lower ADC values in cohorts of 70 and 40 patients, respectively, suggesting higher tumor aggressiveness and cellularity in this subgroup.[42] With a larger cohort, our results support the use of ADC in subgroup differentiation and add that radiomics features can predict the *BRAF* status. In addition, we exploit the entire set of radiomics features, including but not limited to histogram parameters.[16,35,41] We also expand the use of ADC in subgroup differentiation by adding a third non-*BRAF* cohort to the prediction.

RF is an ensemble learning method that combines decision trees and handles various data types, including missing data.[43] In our study, first-order and GLMD classes were among our top discriminative features. First-order statistics describe the distribution of voxel intensities within the image region through commonly used and basic metrics. The mean, kurtosis, and 90th percentile in this class differ among the 3 subgroups. Larger mean, 90th percentile, and kurtosis have been associated with reduced overall survival in glioblastomas.[44] In addition, the mean, median, and 90th percentiles among pediatric patients were lower in the *BRAF* V600E subgroup.[35] These metrics reflect the microstructure at the cellular level.[45] In particular, the low diffusivity of *BRAF* V600E-mutant pLGG may be explained by the dense, compact architecture with fiber-rich regions.[46] GLMD quantifies gray-level dependencies in an image, defined as the number of connected voxels in a certain distance dependent on a central voxel. The dependence variance, large dependence emphasis, and large dependence high gray-level emphasis in this class differed among our subgroups. These are the main features quantifying tumor heterogeneity, which might be missed through the human eyes on MR imaging.[47] Texture features have been shown to differ among brain tumors[48] and predict *IDH* status in low-grade gliomas.[49] Also, the GLMD was the main feature class among the top discriminative features in *KIAA1549-BRAF* fusion and *BRAF* V600E mutation tumors,[17] reflecting the molecular and histologic differences of these tumors.[50]

In our study, tumor location (supra- versus infratentorial) was the most important clinical discriminative feature across the experiments. Many studies support this finding,[9,16,17,35] because *KIAA1549-BRAF* fusion is more often described in the posterior fossa and *BRAF* V600E mutation in the cerebral hemispheres and diencephalon.[35] Sex and age were not significantly different among groups.[16] Other features have also been reported, such as ill-defined margins[35] and a higher number of cystic components.[41] However, the significance of these findings varies in the literature. Ramaglia et al,[41] for instance, did not find significant differences in tumor margins, the presence of hemorrhage/calcification, and contrast enhancement among *BRAF* subgroups in a cohort of 56 participants. Conversely, Shrot et al[35] showed that *KIAA1549-BRAF* fusion tumors had significantly better-defined margins compared with *BRAF* V600E mutation tumors and that *BRAF* subgroups showed more cystic components than the NF1 subgroup in a cohort of 51 participants.

Wagner et al[17] trained and validated the radiomics features of FLAIR sequences to predict *BRAF* status in 115 patients with pLGGs, achieving an AUC of 0.85 on the external validation data set. Similarly, Xu et al[51] extracted features from FLAIR sequences in a cohort of 113 pediatric patients, building a model with a test set AUC of 0.87. We believe that the lower AUC for the ADC values in our study is because we expanded the cohort to include rare subtypes and compared each group versus the rest 3 times. In addition, FLAIR sequences show better margins and facilitate semiautomatic segmentation with good reproducibility.[18] Finally,

pLGGs are heterogeneous neoplasms, and FLAIR sequences may better depict this heterogeneity, including cystic and solid components, margins, and the range of signal changes.[17]

In this study, we noted that the prediction of the *KIAA1549-BRAF* fusion cohort achieved the highest AUC in the per-class analysis. This may be, in part, explained by the larger number of cases in this cohort. In addition, the heterogeneity of histopathologically defined entities was lower in this cohort compared with the other 2 cohorts. Most cases are PA. While it is conceivable to assume that the driver behind this prediction is histopathologic rather than molecular, we also noted that the predictive performance of our algorithm remained high with the other 2 cohorts in the per-class analysis. In contrast to the *KIAA1549-BRAF* fusion cohort, those cohorts were heterogeneous with respect to histopathology. Therefore, we speculate that radiomics can extract predictive information from ADC maps beyond histopathology.

Our study has limitations that need to be considered when interpreting the results. First, due to the retrospective and bi-institutional nature, there was heterogeneity in the DWI sequence acquisition, including using different imaging parameters, field strengths, and scanner vendors. The incorporation of heterogeneous training and testing data was previously shown to be an important component in the development of a robust and predictive ML model. In fact, training of heterogeneous imaging data might increase the generalizability of our findings.[52] Second, our study segmented only ADC images. Incorporating additional sequences could further increase the model performance. Third, we opted to merge the 2 cohorts rather than keep them separated due to an imbalanced distribution of the third class (non-*BRAF*). Fourth, the larger number of cases of *KIAA1549-BRAF* fusion tumors may partially explain the higher AUC among the "fusion versus the rest" per-class analysis. Last, although our study cohort is one of the largest PLGNT cohorts to date, we did not analyze the predictive performance of radiomics features in the subgroup-specific determination of histopathologically defined tumors across molecular markers. Large international MR imaging data sets are necessary for robust subanalyses.

CONCLUSIONS

We explored the feasibility of radiomics features to predict *BRAF* status in PLGNT using ADC-based MR images in a bi-institutional cohort. The optimal RF model included a combination of clinical and radiomic features and achieved diagnostic accuracy. In particular, the highest accuracy was achieved to identify the *KIAA1549-BRAF* fusion tumor subgroup. Differentiating these molecular subgroups in PLGNT is paramount for newer target therapies.[42] Future investigations with additional imaging sequences, such as T2WI and contrast-enhanced T1WI, may improve prediction accuracy.

Disclosure forms provided by the authors are available with the full text and PDF of this article at www.ajnr.org.

REFERENCES

1. Ostrom QT, Price M, Neff C, et al. **CBTRUS Statistical Report: Primary Brain and Other Central Nervous System Tumors Diagnosed in the United States in 2015-2019.** *Neuro Oncol* 2022;24:v1–95 CrossRef Medline

2. Ryall S, Tabori U, Hawkins C. **Pediatric low-grade glioma in the era of molecular diagnostics.** *Acta Neuropathol Commun* 2020;8:30 CrossRef Medline

3. Bale TA, Rosenblum MK. **The 2021 WHO Classification of Tumors of the Central Nervous System: an update on pediatric low-grade gliomas and glioneuronal tumors.** *Brain Pathol* 2022;32:e13060 CrossRef Medline

4. Plant-Fox AS, O'Halloran K, Goldman S. **Pediatric brain tumors: the era of molecular diagnostics, targeted and immune-based therapeutics, and a focus on long term neurologic sequelae.** *Curr Probl Cancer* 2021;45:100777 CrossRef Medline

5. Armstrong GT, Conklin HM, Huang S, et al. **Survival and long-term health and cognitive outcomes after low-grade glioma.** *Neuro Oncol* 2011;13:223–34 CrossRef Medline

6. AlRayahi J, Zapotocky M, Ramaswamy V, et al. **Pediatric brain tumor genetics: what radiologists need to know.** *RadioGraphics* 2018;38:2102–22 CrossRef Medline

7. Chalil A, Ramaswamy V. **Low-grade gliomas in children.** *J Child Neurol* 2016;31:517–22 CrossRef Medline

8. Engelhardt S, Behling F, Beschorner R, et al. **Frequent FGFR1 hotspot alterations in driver-unknown low-grade glioma and mixed neuronal-glial tumors.** *J Cancer Res Clin Oncol* 2022;148:857–66 CrossRef Medline

9. Bag AK, Chiang J, Patay Z. **Radiohistogenomics of pediatric low-grade neuroepithelial tumors.** *Neuroradiology* 2021;63:1185–213 CrossRef Medline

10. Grob ST, Nobre L, Campbell KR, et al. **Clinical and molecular characterization of a multi-institutional cohort of pediatric spinal cord low-grade gliomas.** *Neurooncol Adv* 2020;2:vdaa103 CrossRef Medline

11. Mhatre R, Sugur HS, Nandeesh BN, et al. **MN1 rearrangement in astroblastoma: study of eight cases and review of literature.** *Brain Tumor Pathol* 2019;36:112–20 CrossRef Medline

12. Moreira DC, Lam CG, Bhakta N, et al. **Tackling pediatric low-grade gliomas: a global perspective.** *JCO Glob Oncol* 2023;9:e2300017 CrossRef Medline

13. Vagvala S, Guenette JP, Jaimes C, et al. **Imaging diagnosis and treatment selection for brain tumors in the era of molecular therapeutics.** *Cancer Imaging* 2022;22:19 CrossRef Medline

14. Ryall S, Zapotocky M, Fukuoka K, et al. **Integrated molecular and clinical analysis of 1,000 pediatric low-grade gliomas.** *Cancer Cell* 2020;37:569–83.e5 CrossRef Medline

15. Nobre L, Zapotocky M, Ramaswamy V, et al. **Outcomes of BRAF V600E pediatric gliomas treated with targeted BRAF inhibition.** *JCO Precis Oncol* 2020;4:561–71 CrossRef Medline

16. Trasolini A, Erker C, Cheng S, et al. **MR imaging of pediatric low-grade gliomas: pretherapeutic differentiation of BRAF V600E mutation, BRAF musion, and wild-type tumors in patients without neurofibromatosis-1.** *AJNR Am J Neuroradiol* 2022;43:1196–201 CrossRef Medline

17. Wagner MW, Hainc N, Khalvati F, et al. **Radiomics of pediatric low-grade gliomas: toward a pretherapeutic differentiation of BRAF-mutated and BRAF-fused tumors.** *AJNR Am J Neuroradiol* 2021;42:759–65 CrossRef Medline

18. Madhogarhia R, Haldar D, Bagheri S, et al. **Radiomics and radiogenomics in pediatric neuro-oncology: a review.** *Neurooncol Adv* 2022;4:vdac083 CrossRef Medline

19. Zhang M, Wong SW, Wright JN, et al. **MRI radiogenomics of pediatric medulloblastoma: a multicenter study.** *Radiology* 2022;304:406–16 CrossRef Medline

20. Guerrini F, Paolicchi M, Ghio F, et al. **The Droplet Digital PCR: a new valid molecular approach for the assessment of B-RAF V600E mutation in hairy cell leukemia.** *Front Pharmacol* 2016;7:363 CrossRef Medline

21. Fedorov A, Beichel R, Kalpathy-Cramer J, et al. **3D slicer as an image computing platform for the quantitative imaging network.** *Magn Reson Imaging* 2012;30:1323–41 CrossRef Medline

22. Parmar C, Velazquez ER, Leijenaar R, et al. **Robust radiomics feature quantification using semiautomatic volumetric segmentation.** *PloS One* 2014;9:e102107 CrossRef Medline

23. Li J, Liu S, Qin Y, et al. **High-order radiomics features based on T2 FLAIR MRI predict multiple glioma immunohistochemical features: a more precise and personalized gliomas management.** *PLoS One* 2020;15:e0227703 CrossRef Medline

24. Tustison NJ, Avants BB, Cook PA, et al. **N4ITK: improved N3 bias correction.** *IEEE Trans Med Imaging* 2010;29:1310–20 CrossRef Medline

25. Aerts HJ, Velazquez ER, Leijenaar RTH, et al. **Decoding tumour phenotype by noninvasive imaging using a quantitative radiomics approach.** *Nat Commun* 2014;5:4006–09 CrossRef Medline

26. Chaddad A, Kucharczyk MJ, Daniel P, et al. **Radiomics in glioblastoma: current status and challenges facing clinical implementation.** *Front Oncol* 2019;9:374 CrossRef Medline

27. Eun Park J, Sung Kim H. **Radiomics as a quantitative imaging biomarker: practical considerations and the current standpoint in neuro-oncologic studies.** *Nucl Med Mol Imaging* 2018;52:99–108 CrossRef Medline

28. Breiman L. **Bagging predictors.** *Mach Learn* 1996;24:123–40 CrossRef

29. Wagner M, Namdar K, Alqabbani A, et al. **Dataset size sensitivity analysis of machine learning classifiers to differentiate molecular markers of pediatric low-grade gliomas based on MRI.** *Research Square* 2021 Sept 17 [Epub ahead of print] CrossRef

30. Faulkner C, Ellis HP, Shaw A, et al. **BRAF fusion analysis in pilocytic astrocytomas: KIAA1549-BRAF 15-9 fusions are more frequent in the midline than within the cerebellum.** *J Neuropathol Exp Neurol* 2015;74:867–72 CrossRef Medline

31. Di Nunno V, Gatto L, Tosoni A, et al. **Implications of BRAF V600E mutation in gliomas: molecular considerations, prognostic value and treatment evolution.** *Front Oncol* 2022;12:1067252 CrossRef Medline

32. Koh DM, Collins DJ. **Diffusion-weighted MRI in the body: applications and challenges in oncology.** *AJR Am J Roentgenol* 2007;188:1622–35 CrossRef Medline

33. Guo AC, Cummings TJ, Dash RC, et al. **Lymphomas and high-grade astrocytomas: comparison of water diffusibility and histologic characteristics.** *Radiology* 2002;224:177–83 CrossRef Medline

34. Doskaliyev A, Yamasaki F, Ohtaki M, et al. **Lymphomas and glioblastomas: Differences in the apparent diffusion coefficient evaluated with high b-value diffusion-weighted magnetic resonance imaging at 3T.** *Eur J Radiol* 2012;81:339–44 CrossRef Medline

35. Shrot S, Kerpel A, Belenky J, et al. **MR imaging characteristics and ADC histogram metrics for differentiating molecular subgroups of pediatric low-grade gliomas.** *AJNR Am J Neuroradiol* 2022;43:1356–62 CrossRef Medline

36. Kolossváry M, Kárády J, Kikuchi Y, et al. **Radiomics versus visual and histogram-based assessment to identify atheromatous lesions at coronary CT angiography: an ex vivo study.** *Radiology* 2019;293:89–96 CrossRef Medline

37. Capobianco E, Deng J. **Radiomics at a glance: a few lessons learned from learning approaches.** *Cancers (Basel)* 2020;12:2453 CrossRef Medline

38. Namdar K, Wagner MW, Ertl-Wagner BB, Khalvati F. **Open-radiomics: a collection of standardized datasets and a technical protocol for reproducible radiomics machine learning pipelines.** *arXiv* July 29 [Epub ahead of print]. https://arxiv.org/abs/2207.14776

39. Lam LH, Do DT, Diep DT, et al. **Molecular subtype classification of low-grade gliomas using magnetic resonance imaging-based radiomics and machine learning.** *NMR Biomed* 2022;35:e4792 CrossRef Medline

40. Manoharan N, Liu KX, Mueller S, Haas-Kogan DA, Bandopadhayay P. **Pediatric low-grade glioma: Targeted therapeutics and clinical trials in the molecular era.** *Neoplasia* 2023;36:100857 CrossRef Medline

41. Ramaglia A, Tortora D, Mankad K, et al. **Role of diffusion weighted imaging for differentiating cerebral pilocytic astrocytoma and ganglioglioma BRAF V600E-mutant from wild type.** *Neuroradiology* 2020;62:71–80 CrossRef Medline

42. Kan P, Liu JK, Hedlund G, et al. **The role of diffusion-weighted magnetic resonance imaging in pediatric brain tumors.** *Childs Nerv Syst* 2006;22:1435–39 CrossRef Medline

43. Erickson BJ, Korfiatis P, Akkus Z, et al. **Machine learning for medical imaging.** *Radiographics* 2017;37:505–15 CrossRef Medline

44. Li Y, Kim MM, Wahl DR, et al. **Survival prediction analysis in glioblastoma with diffusion kurtosis imaging.** *Front Oncol* 2021;11:690036 CrossRef Medline

45. Wu CC, Jain R, Radmanesh A, et al. **Predicting genotype and survival in glioma using standard clinical MR imaging apparent diffusion coefficient images: a pilot study from The Cancer Genome Atlas.** *AJNR Am J Neuroradiol* 2018;39:1814–20 CrossRef Medline

46. Ho CY, Mobley BC, Gordish-Dressman H, et al. **A clinicopathologic study of diencephalic pediatric low-grade gliomas with BRAF V600 mutation.** *Acta Neuropatho* 2015;130:575–85 CrossRef Medline

47. Cho HH, Lee SH, Hak Kim J, et al. **Classification of the glioma grading using radiomics analysis.** *PeerJ* 2018;6:e5982 CrossRef Medline

48. Widhiarso W, Yohannes Y, Prakarsah C. **Brain tumor classification using gray level co-occurrence matrix and convolutional neural network.** *Indonesian J Electron Instrum Syst* 2018;8:179–90 CrossRef

49. Chekouo T, Mohammed S, Rao A. **A Bayesian 2D functional linear model for gray-level co-occurrence matrices in texture analysis of lower grade gliomas.** *Neuroimage Clin* 2020;28:102437 CrossRef Medline

50. Zachariah RM, Priya PS, Pendem S. **Classification of low- and high-grade gliomas using radiomic analysis of multiple sequences of MRI brain.** *J Cancer Res Ther* 2023;19:435–46 CrossRef Medline

51. Xu J, Lai M, Li S, et al. **Radiomics features based on MRI predict BRAF V600E mutation in pediatric low-grade gliomas: a noninvasive method for molecular diagnosis.** *Clin Neurol Neurosurg* 2022;222:107478 CrossRef Medline

52. Mårtensson G, Ferreira D, Granberg T, et al. **The reliability of a deep learning model in clinical out-of-distribution MRI data: amulticohort study.** *Med Image Anal* 2020;66:101714 CrossRef Medline